ADVANCES IN ATMOSPHERIC SCIENCES, VOL. 33, JANUARY 2016, 121–134

Revisiting the Second EOF Mode of Interannual Variation in Summer Rainfall over East China

Zhongda LIN*[1], Qin SU[2], and Riyu LU[1]

[1]*State Key Laboratory of Numerical Modeling for Atmospheric Sciences and Geophysical Fluid Dynamics, Institute of Atmospheric Physics, Chinese Academy of Sciences, Beijing* 100029

[2]*Department of Atmospheric Sciences, Yunnan University, Kunming* 650091

(Received 10 January 2015; revised 5 June 2015; accepted 9 July 2015)

ABSTRACT

The second EOF (EOF2) mode of interannual variation in summer rainfall over East China is characterized by inverse rainfall changes between South China (SC) and the Yellow River–Huaihe River valleys (YH). However, understanding of the EOF2 mode is still limited. In this study, the authors identify that the EOF2 mode physically depicts the latitudinal variation of the climatological summer-mean rainy belt along the Yangtze River valley (YRRB), based on a 160-station rainfall dataset in China for the period 1951–2011. The latitudinal variation of the YRRB is mostly attributed to two different rainfall patterns: one reflects the seesaw (SS) rainfall changes between the YH and SC (SS pattern), and the other features rainfall anomalies concentrated in SC only (SC pattern). Corresponding to a southward shift of the YRRB, the SS pattern, with above-normal rainfall in SC and below-normal rainfall in the YH, is related to a cyclonic anomaly centered over the SC–East China Sea region, with a northerly anomaly blowing from the YH to SC; while the SC pattern, with above-normal rainfall in SC, is related to an anticyclonic anomaly over the western North Pacific (WNP), corresponding to an enhanced southwest monsoon over SC. The cyclonic anomaly, related to the SS pattern, is induced by a near-barotropic eastward propagating wave train along the Asian upper-tropospheric westerly jet, originating from the mid–high latitudes of the North Atlantic. The anticyclonic anomaly, for the SC pattern, is related to suppressed rainfall in the WNP.

Key words: Yangtze River rainy belt, East China summer rainfall, seesaw pattern, South China pattern, western North Pacific subtropical high, extratropical wave train

Citation: Lin, Z. D., Q. Su, and R. Y. Lu, 2016: Revisiting the Second EOF Mode of Interannual Variation in Summer Rainfall over East China. *Adv. Atmos. Sci.*, **33**(1), 121–134, doi: 10.1007/s00376-015-5010-1.

1. Introduction

Summer rainfall in East China exhibits a strong year-to-year variability due to its typical monsoon climate, which leads to frequent flood and drought. Understanding the year-to-year variations of summer rainfall, therefore, is essential and many works have been devoted to this topic (Lau et al., 2000; Wang et al., 2001; Huang et al., 2003; Lu, 2004; Ding and Chan, 2005; Shen et al., 2011; Su et al., 2014).

EOF analysis is the most common approach to investigate variations in summer rainfall in East China. Most such studies have been summarized in the recent works of Ye and Lu (2012) and Huang et al. (2012). Their results showed that the first EOF (EOF1) mode of summer rainfall features a meridional tripole pattern in East China, with increased rainfall located in the middle–lower reaches of the Yangtze River valley and decreased rainfall to the both north and south (He and Li, 1992; Zhu and Chen, 1992; Shen and Lau, 1995; Zou and Ni, 1998; Weng et al., 1999; You et al., 2003; Zhou and Yu, 2005; Chen et al., 2006; Huang et al., 2006, 2007, 2012; Ye and Lu, 2012). This EOF1 mode is associated with the "Pacific–Japan (PJ)" teleconnection proposed by Nitta (1987) or the "East Asia–Pacific (EAP)" teleconnection, proposed by Huang and Sun (1992), and a Rossby wave train over the midlatitudes of continental Eurasia (Huang et al., 2007).

The second EOF (EOF2) mode is characterized by rainfall anomalies with opposite sign in South China (SC) and the Yellow River–Huaihe River valleys (YH) (Zhu and Chen, 1992; Shen and Lau, 1995; Weng et al., 1999; You et al., 2003; Zhou and Yu, 2005; Chen et al., 2006; Huang et al., 2007, 2012; Ye and Lu, 2012). The corresponding principal component (PC2) shows a decadal shift around the early 1990s, consistent with significantly enhanced rainfall in SC after 1992 (Wu et al., 2010).

Some previous studies investigated circulation anomalies associated with the EOF2 mode (e.g., Zhou and Yu, 2005; Han and Zhang, 2009). The negative phase of the EOF2 mode, with increased rainfall in the YH and decreased rain-

* Corresponding author: Zhongda LIN
Email: zdlin@mail.iap.ac.cn

fall in SC, is related to a northwestward extension of the western North Pacific subtropical high (WNPSH) and an eastward shift of the upper jet stream (Zhou and Yu, 2005). On the contrary, the positive phase of the EOF2 mode is associated with a southwestward extension of the WNPSH (Han and Zhang, 2009). Consequently, the subtropical southwest moisture transport in the west of the WNPSH converges with midlatitude moisture transport over the YH in the negative phase (Zhou and Yu, 2005) and over SC in the positive phase (Han and Zhang, 2009). Indeed, these studies concentrated on the decadal change of the EOF2 mode around the early 1990s; similar circulation anomalies associated with the decadal change of summer rainfall in SC after 1992 have also been identified (Wu et al., 2010).

In addition to the significant decadal change around the early 1990s, the EOF mode with opposite rainfall change between the YH and SC has also been identified from interannual variations of summer rainfall in East China (Ye and Lu, 2012). Ye and Lu (2012) revealed that this mode accounts for 10.9% of the total variance of interannual variations of summer rainfall in East China during 1955–2002 and, as the EOF2 mode, is distinguishable from the EOF1 mode. Unfortunately, their results did not show any associated circulation change, so the physical processes involved are still not clear.

The objective of the present study is to investigate the EOF2 mode of summer rainfall in East China on interannual timescales and to discuss the possible underlying mechanisms. The text is organized as follows: Section 2 introduces the data used in the study. In section 3, the first two dominant modes of interannual summer rainfall in East China are obtained based on EOF analysis. In section 4, based on the variation of summer rainfall in the YH and SC, the authors identify two main patterns in the EOF2 mode: one features a seesaw (SS) rainfall change between the YH and SC, and the other with rainfall anomalies concentrated in SC only. The possible mechanisms responsible for the SS and SC pattern are investigated in section 5. Finally, conclusions and discussion are provided in section 6.

2. Data

In this study, the 160-station observed monthly rainfall data in mainland China during 1951–2011, provided by the National Climate Center of the China Meteorological Administration, are used to obtain the first two EOF leading modes in East China. Also used are global precipitation data derived by the Global Precipitation Climatology Project (GPCP) (Huffman et al., 1997; Adler et al., 2003) during 1979–2010, and precipitable water for the entire atmosphere from the National Centers for Environmental Prediction–National Center for Atmospheric Research (NCEP–NCAR) reanalysis data (Kalnay et al., 1996) during 1951–2011. The resolution is $2.5^\circ \times 2.5^\circ$ for both the GPCP data and the NCEP–NCAR reanalysis data. In addition, monthly National Oceanic and Atmospheric Administration ERSST (extended reconstructed sea surface temperature) data (Smith et al., 2008) are also used.

The monthly atmospheric data are from the NCEP–NCAR reanalysis datasets (Kalnay et al., 1996) during 1951–2011, with a horizontal resolution of $2.5^\circ \times 2.5^\circ$ at 17 pressure levels. Also used are the 6-h specific humidity, zonal and meridional wind at the eight pressure levels from 1000 hPa to 300 hPa, and surface pressure data from the NCEP–NCAR reanalysis datasets (Kalnay et al., 1996) for the period 1951–2011. The 6-h data are applied to calculate moisture transport and its divergence. Similar to Chen and Huang (2007), the column moisture flux $\boldsymbol{Q}$ is integrated vertically from 300 hPa to the surface,

$$\boldsymbol{Q} = \frac{1}{g}\int_{300}^{P_s} q\boldsymbol{V}\,dp\ ,$$

and its divergence D is calculated as

$$D = \nabla\cdot\boldsymbol{Q} = \frac{1}{g}\nabla\cdot\int_{300}^{P_s} q\boldsymbol{V}\,dp\ ,$$

where q is specific humidity, p is pressure, and $\boldsymbol{V}$ is the horizontal wind vector including zonal (u) and meridional (v) wind components. The constant g is gravitational acceleration and the variable P_s is atmospheric pressure at the surface. The variables $\boldsymbol{Q}$ and D are first calculated at 6-h temporal resolution, and then their seasonal means are derived. When $D > 0$, moisture flux diverges, acting as a sink of moisture; when $D < 0$, it converges, acting as a source of moisture and favors rainfall.

In this study, summer is defined as June–July–August (JJA). To obtain interannual anomalies, a 9-yr Guassian filter is employed to remove long-term trends and decadal variations of summer rainfall and circulation anomalies.

3. The EOF2 mode of interannual summer rainfall in East China

Figure 1a shows the climatology of summer-mean rainfall in East China east of 105°E and south of 45°N, which includes 108 stations as depicted by black dots. There are two main rainy belts with summer-mean rainfall exceeding 5 mm d^{-1}: the rainy belt along the Yangtze River (YRRB), and along the southeast coast of China. Along these two belts, summer rainfall also exhibits strong interannual variation, with the maximum of standard deviation being larger than 2 mm d^{-1} during 1951–2011 (Fig. 1b).

We perform the EOF analysis on interannual summer rainfall in East China and present the first two EOF modes in Figs. 1c and d. The spatial pattern of rainfall anomalies of the EOF1 mode features increased rainfall in the Yangtze River valley and decreased rainfall over the southeast coast of China (Fig. 1c). It physically depicts a rainfall oscillation between the YRRB and the rainy belt along the southeast coast of China. This mode explains 17% of the total variance. A similar spatial pattern was also obtained in the EOF1 mode of the interannual component of summer rainfall in East China during 1955–2002 by Ye and Lu (2012). Note that the rainfall anomalies in North China are weak and positive, which

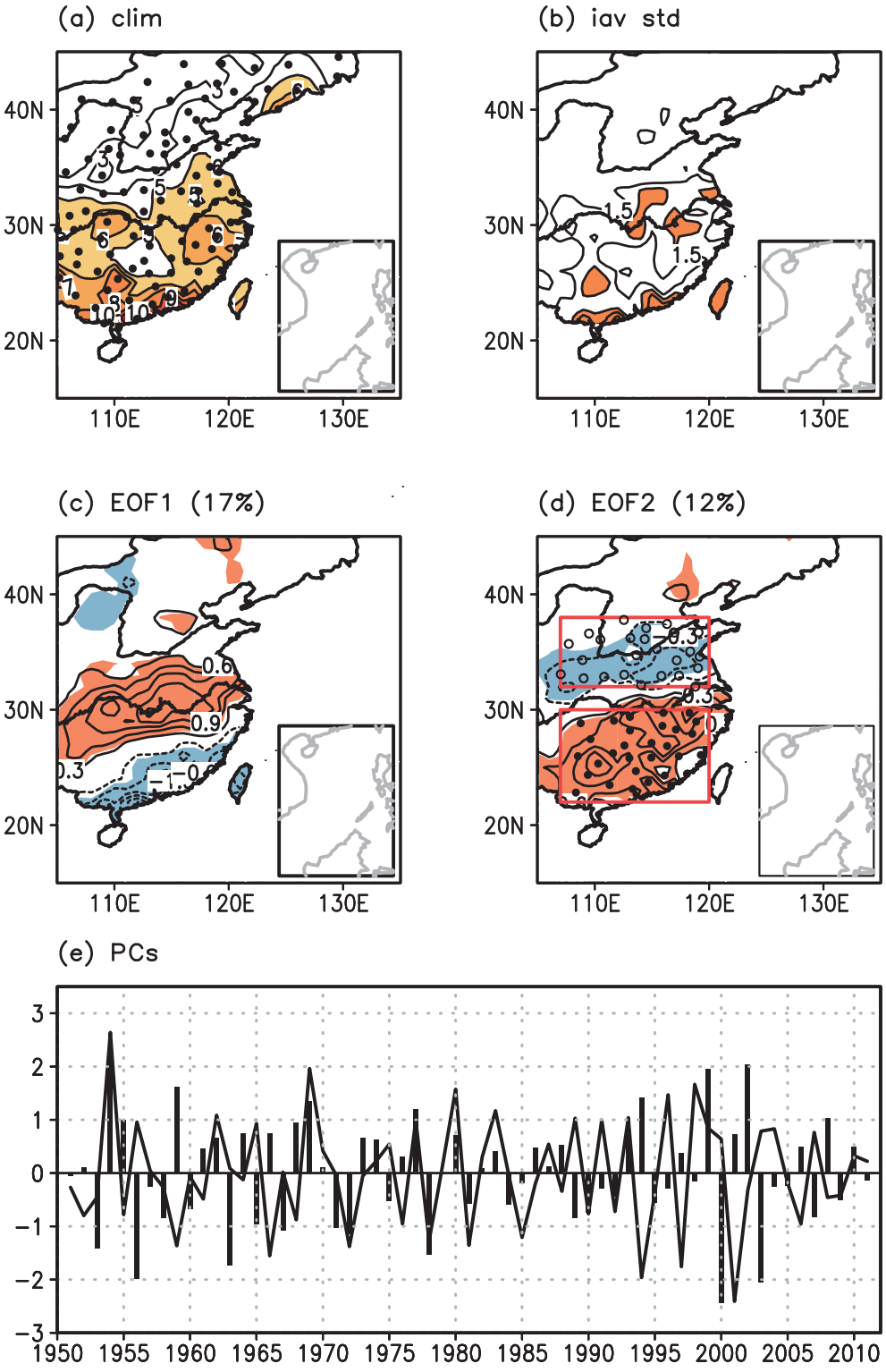

Fig. 1. (a) Climatology and (b) interannual standard deviation of summer rainfall for 1951–2011 in East China. The filled circles depict 108 stations east of 105°E and south of 45°N. The (c) first and (d) second EOF modes of interannual summer rainfall in East China. (e) The normalized PCs corresponding to the first (line) and second (bars) modes. Spatial patterns in (c, d) are shown as regressed anomalies against the corresponding normalized PCs. Shading indicates rainfall exceeding 5 and 2 mm d^{-1} in (a) and (b), respectively, and depicts significant rainfall anomalies at the 95% confidence level in (c, d). The contour interval is 1, 0.5, 0.3 and 0.3 mm d^{-1} in (a–d), respectively. The two regions depicted by the rectangles in (d) are the YH (north region), which includes 25 stations (open circles), and SC (south region), which includes 30 stations (filled circles).

are different from those revealed by Huang et al. (2012) using total rainfall data. This difference is probably due to the effect of opposite decadal variations of summer rainfall between North China and the Yangtze River valley around the late 1970s (Huang et al., 1999; Huang et al., 2012).

The EOF2 mode features inverse rainfall changes between South China (SC) and the Yellow River–Huaihe River valleys (YH) (Fig. 1d). This mode accounts for 12% of the total interannual variance of summer rainfall in East China, which is distinguishable from the EOF1 mode (17%) and from the third EOF mode (8%) in terms of the criterion of North et al. (1982). Moreover, the maximum of interannual variance of summer rainfall explained by the EOF2 mode is more than 50% in SC (Fig. 2a), and that of total variance is more than 40% (Fig. 2b). As for the YH summer rainfall, this mode explains the maximum of more than 30% of its interannual variance (Fig. 2a) and 20% of total variance (Fig. 2b). The area-averaged explicable fractions of interannual variance are larger than 20% and 10% in SC and the YH, respectively, and those of total variance larger than 17% and 8%.

To reveal the physical meaning of the EOF2 mode, 19 positive-phase cases, corresponding to the associated principal component (PC2) being larger than 0.5, and 20 negative-phase cases, with the corresponding PC2 being smaller than −0.5, are chosen (Table 1). Based on the 39 cases, interannual rainfall anomalies (Figs. 3a and d) and total rainfall (Figs. 3b and e) in summer are then composited. Rainfall increases in SC and decreases in the YH in the positive phase of the EOF2 mode (Fig. 3a). Accordingly, the YRRB is located to the south of the Yangtze River (Fig. 3b). In the negative phase, rainfall decreases in SC and increases in the YH (Fig. 3d), and the YRRB moves northward to north of the Yangtze River (Fig. 3e). Meanwhile, the rainy belt along the southeast of China remains in both the positive (Fig. 3b) and negative (Fig. 3e) phases. The result indicates that the EOF2 mode depicts a meridional shift of the summer YRRB. Figures 3c and f show total summer rainfall (shading) and their interannual anomalies (contours) in two cases of the positive and negative phases of the EOF2 mode, respectively. The YRRB shifted southward in 1999 in the positive phase (Fig. 3c) and northward in 2003 in the negative phase (Fig. 3f), consistent with the composite results. It is also noted that the interannual rainfall anomalies in the YH are weaker than those in SC in the composite results (Figs. 3a and d), which is due to the effect of more than one third of cases with rainfall anomalies being concentrated mainly in SC only, in addition to the cases with inverse rainfall variation between the YH and SC, related to the EOF2 mode, identified in the next section.

To further reveal the relationship between the meridional shift of the YRRB and rainfall variations in the YH and SC, two regions (32°–38°N, 107°–120°E) and (22°–30°N, 107°–120°E), as depicted by the two boxes in Fig. 1d, are chosen to represent the YH and SC regions, respectively. The YH box includes 25 stations and the SC box includes 30 stations.

Table 1. Years with a strong EOF2 mode of interannual summer rainfall in East China. The years with the PC2 value being larger (smaller) than 0.5 (−0.5) are chosen for the positive (negative) phase.

	Year
Positive phase (19 years)	1954, 1955, 1959, 1962, 1964, 1966, 1968, 1969, 1973, 1974, 1977, 1980, 1988, 1993, 1994, 1999, 2001, 2002, 2008
Negative phase (20 years)	1953, 1956, 1958, 1960, 1963, 1965, 1967, 1971, 1972, 1975, 1978, 1981, 1984, 1989, 1990, 1995, 2000, 2003, 2007, 2009

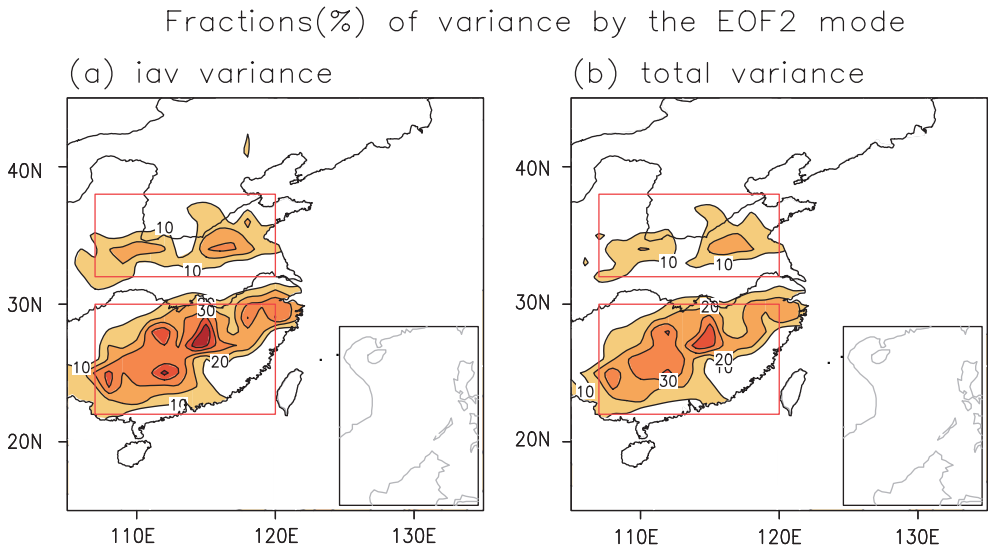

Fig. 2. Fractions (%) of (a) interannual and (b) total variance of summer rainfall explained by the EOF2 mode.

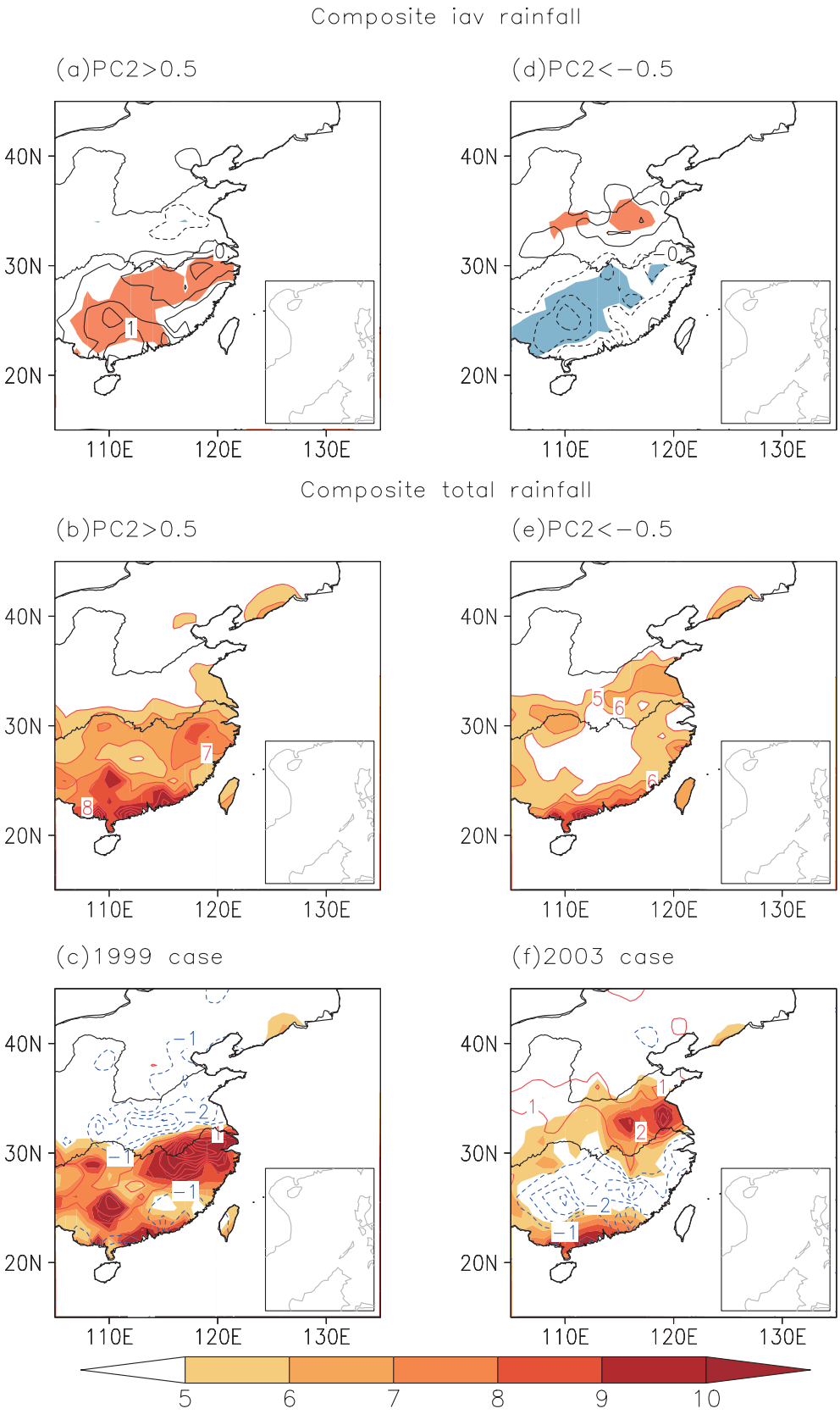

Fig. 3. Composite results of (a, d) interannual summer rainfall anomalies and (b, e) total rainfall in East China, and (c, f) case results of total summer rainfall (shading) and interannual anomalies (contours), in the (a–c) positive and (d–f) negative phases of the EOF2 mode. Shading indicates statistical significance at the 95% confidence level in (a, d) and depicts rainfall exceeding 5 mm d^{-1} in (b, c, e, f) (scale bar at the bottom). The contour interval is 0.5 mm d^{-1} in (a, d) and 1 mm d^{-1} in (b, c, e, f).

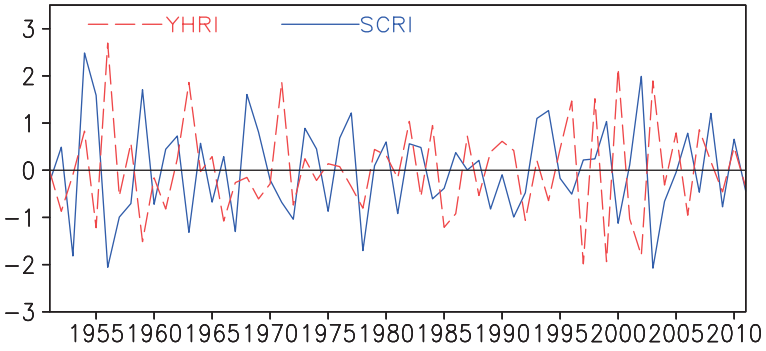

Fig. 4. Normalized time series of the rainfall indices of SC (SCRI) and the YH (YHRI). The SCRI is defined as interannual summer rainfall anomalies of the 30-station mean in SC and the YHRI of the 25-station mean in the YH, as shown in Fig. 1d.

Accordingly, the YH rainfall index (YHRI) is defined as the 25-station mean rainfall and the SC rainfall index (SCRI) as the 30-station mean rainfall. Figure 4 shows time series of the two rainfall indices. The correlation coefficients of the PC2 with the SCRI and YHRI are 0.93 and −0.57, respectively, both significant at the 99% confidence level. In addition, the YHRI is also significantly correlated with the SCRI, with a correlation coefficient of −0.41, suggesting the interannual variation of the SC summer rainfall is, at least partially, related to that of the YH summer rainfall. A southward shift of the YRRB is related to a significant rainfall increase in SC and decrease in the YH.

4. Identification of the SS and SC patterns related to the EOF2 mode

The EOF2 mode, as identified in the last section, which depicts a meridional shift of the YRRB, is associated with the rainfall variations in both the YH and SC. In this section, the EOF2-mode cases are further classified into nine different groups based on the combined distribution of the normalized SCRI and YHRI (Fig. 5). A red dot depicts a strong, positive EOF2-mode year, with the PC2 value being larger than 0.5, and a blue dot represents a strong, negative EOF2-mode year, with the PC2 value being less than −0.5. The 39 strong EOF2-mode years are located mainly in four phases: Phase 1, with strong, positive rainfall anomalies in SC and strong, negative rainfall anomalies in the YH; Phase 4, which is the inverse of Phase 1; Phase 2, with strong, positive rainfall anomalies in SC and normal rainfall in the YH; and Phase 3, which is opposite to Phase 2.

The phase distribution of the strong EOF2-mode years is summarized in detail in Table 2. There are six and seven years in Phases 1 and 4, and eight years in both Phases 2 and 3. The summed number of years in these four phases is 29, which accounts for approximately three quarters of the total 39 strong EOF2-mode years. Note that the differences between Phases 1 and 2 and between Phases 3 and 4 are whether or not rainfall anomalies in the YH are strong. The Student's *t*-test is used to obtain the statistical significance for the following composite results.

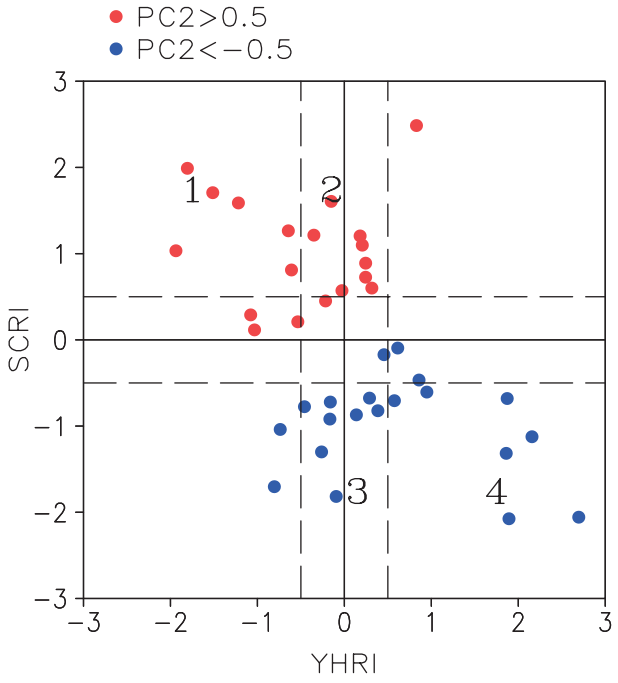

Fig. 5. Phase distribution of the strong EOF2-mode years based on the normalized YHRI and SCRI. A positive (negative) EOF2-mode year with the PC2 value being larger (smaller) than 0.5 (−0.5), is depicted by red (blue) dots.

Figure 6 shows the composite interannual rainfall anomalies in the four phases. Phase 1 features an SS-like pattern, with increased rainfall in SC and decreased rainfall in the YH (Fig. 6a). The amounts of rainfall anomalies in these two regions are nearly equivalent. An opposite pattern is identified in Phase 4, with reduced rainfall in SC and enhanced rainfall in the YH (Fig. 6b). Composite differences of rainfall anomalies between these two phases show significant, positive anomalies in SC and significant, negative anomalies in the YH (Fig. 6c), resembling the EOF2 mode (Fig. 1d). To distinguish from the EOF2 mode, this pattern is, hereafter, referred to as the SS pattern. Phases 1 and 4 then depict the positive and negative phases of the SS pattern, respectively.

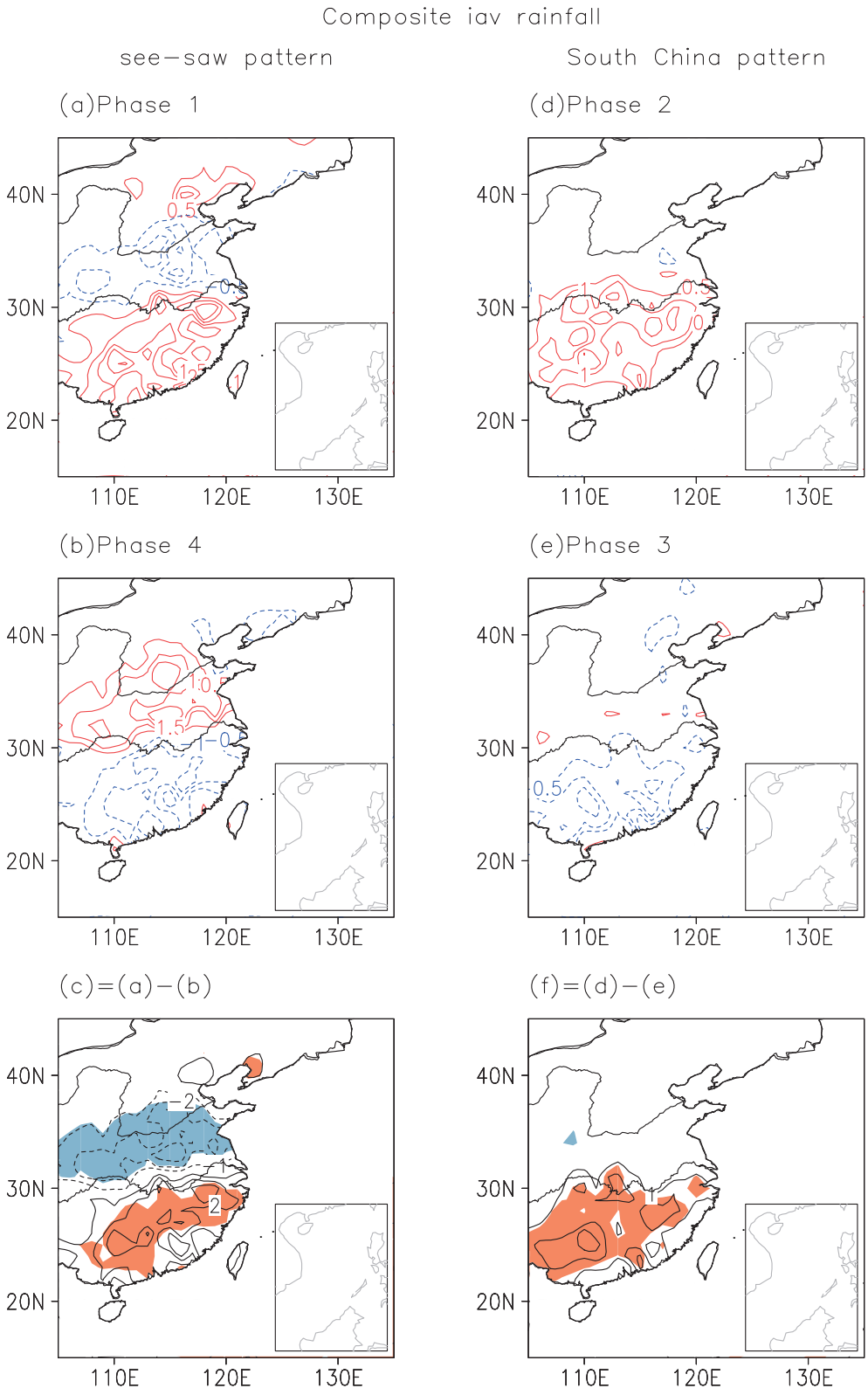

Fig. 6. Composite interannual summer rainfall anomalies in East China based on (a, b, d, e) four categories of the EOF2-mode cases in Table 2 and (c, f) their difference. The spatial pattern of rainfall anomalies is referred to as the (a–c) SS pattern and (d–f) SC pattern. Phases 1 and 4 (2 and 3) represent the positive and negative phases of the SS (SC) pattern, respectively. Shading represents statistically significant anomalies at the 95% confidence level in (c, f), and the contour interval is 0.5 mm d^{-1} in (a, b, d, e) and 1 mm d^{-1} in (c, f).

Table 2. Phase distribution of the strong EOF2-mode years based on the YHRI and SCRI. The years underlined are in the negative phase of the EOF2 mode and the other years are in the positive phase.

	YHRI $\leqslant -0.5$	$-0.5 <$ YHRI < 0.5	YHRI $\geqslant 0.5$
SCRI $\geqslant 0.5$	1955, 1959, 1969, 1994, 1999, 2002	1962, 1964, 1968, 1973, 1977, 1980, 1993, 2008	1954
$-0.5 <$ SCRI < 0.5	1966, 1988, 2001	1974, 1995	1997, 2007
SCRI $\leqslant -0.5$	1972, 1978	1953, 1960, 1965, 1967, 1975, 1981, 1989, 2009	1956, 1958, 1963, 1971, 1984, 2000, 2003

In Phase 2 rainfall is also increased in SC (Fig. 6d), similar to that in Phase 1 (Fig. 6a). However, there are no strong rainfall anomalies in the YH in Phase 2, in contrast with those in Phase 1. In Phase 3 rainfall is reduced in SC (Fig. 6e), opposite to that in Phase 2 (Fig. 6d). Their difference shows significant, positive rainfall anomalies concentrated in SC and no significant anomalies in the YH (Fig. 6f). This pattern is named the SC pattern, in which Phases 2 and 3 represent its positive and negative phases, respectively.

In the above analysis the EOF2-mode cases are then mainly classified into two patterns: the SS pattern and the SC pattern. The SS pattern reflects the fact that interannual variations of rainfall in SC are closely related to those in the YH, while the SC pattern represents rainfall varying locally over SC. The two cases in 1999 and 2003, as shown in Figs. 3c and f, distributed in Phases 1 and 4 (Table 2) respectively, are the SS-pattern cases with relatively equivalent amounts of interannual rainfall anomalies in both the YH and SC. On the other hand, the combination of the SS- and SC-pattern cases, leads to stronger interannual rainfall anomalies in SC than the YH in the composite results, as shown in Figs. 3a and d.

But do both the SS and SC patterns lead to a meridional shift of the YRRB, the same as that in the composite results in Fig. 3? Figure 7 shows the latitudinal variation of the YRRB averaged between 107°E and 120°E for the SS and SC patterns, separately. The mean location of the YRRB moves from 29°N in the positive phase of the SS pattern to 33°N in the negative phase (Fig. 7a), and in the SC pattern from 29°N to 31°N (Fig. 7b). The SS and SC patterns both induce a meridional shift of the YRRB, though the YRRB moves more northward in the negative phase of the SS pattern, due to the contribution of both the decreased rainfall in SC and increased rainfall in the YH, compared to the SC pattern related to decreased rainfall in SC only.

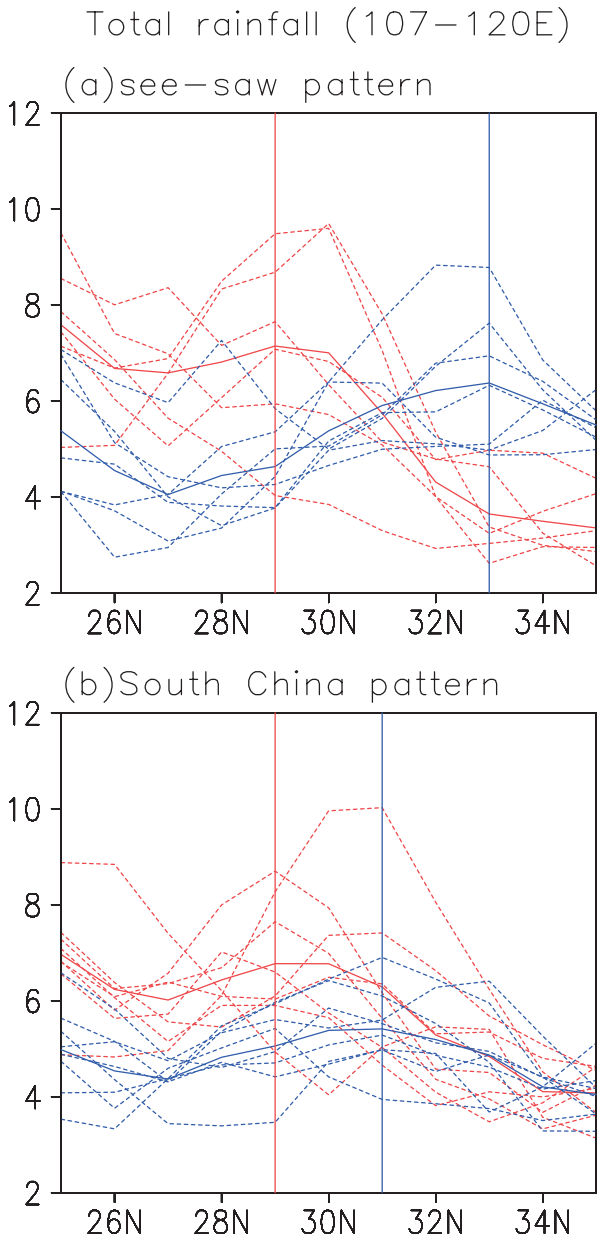

Fig. 7. Latitudinal variation of total summer rainfall (units: mm d^{-1}) averaged zonally between 107°E and 120°E for each case (dotted line) and their mean (solid line) of the (a) SS and (b) SC pattern. Red lines represent the positive phase and blue lines the negative phase. The vertical solid lines indicate the latitude of the maximum of composite mean total rainfall, the location of the summer rainy belt in East China, in the positive (red) and negative (blue) phases.

5. Underlying mechanisms

5.1. *Local anomalies associated with the SS and SC patterns*

To reveal the circulation anomalies responsible, Fig. 8 shows the composite results of horizontal wind anomalies at 850 hPa in summer associated with the SS and SC patterns, separately. Clearly, the SS pattern, with increased rainfall in SC and decreased rainfall in the YH in the positive phase (Phase 1), is significantly associated with a cyclonic anomaly over SC and the neighboring East China Sea (Fig. 8a). In

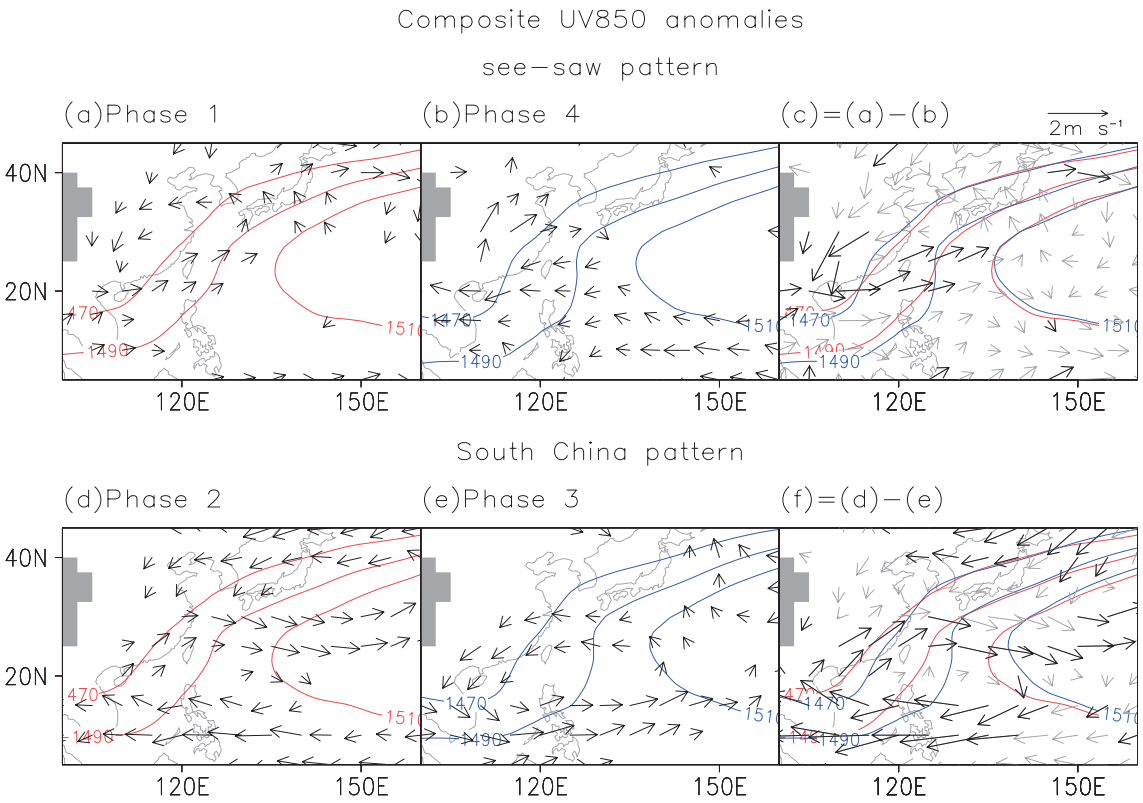

Fig. 8. As in Fig. 6 but for the composite results of the WNPSH (contours) and interannual horizontal wind anomalies at 850 hPa (vectors). The WNPSH is depicted by geopotential height (units: gpm) at 850 hPa, with the contours of 1470, 1490 and 1510. Statistically significant wind anomalies at the 95% confidence level are plotted with bold vectors in (c, f). The units for wind are given in the top-right corner of (c). The effect of the topography is masked by grey shading.

contrast, an anticyclonic anomaly is identified in the negative phase (Phase 4, Fig. 8b). Their difference shows a significant cyclonic anomaly over the SC–East China Sea region (Fig. 8c). The cyclone-induced northerly anomaly blows from the YH to SC, which weakens the climatological southwest summer monsoon in East Asia. Subsequently, the weakened monsoon airflow suppresses northward moisture transport. The latter diverges over the YH and converges over SC (Fig. 9a). Rainfall decreases in the YH and increases in SC, concurrent with ascending motion anomalies over SC and descending motion anomalies over the YH (Fig. 9b).

For the SC pattern, the increased rainfall in SC is related to an anticyclonic anomaly over the northern South China Sea (SCS) and the Philippine Sea in the positive phase (Phase 2, Fig. 8d), and the decreased rainfall in SC is associated with a cyclonic anomaly in the negative phase (Phase 3, Fig. 8e). Their difference is characterized by a significant anticyclonic anomaly (Fig. 8f), corresponding to the westward extension of the western North Pacific subtropical high (WNPSH). Due to the southerly anomaly in the west of the anticyclonic anomaly, more moisture is transported to SC (Fig. 9c), together with ascending motion anomalies (Fig. 9d), enhancing rainfall over SC.

In summary, in the positive phase, the SS-pattern rainfall anomalies are induced by the cyclonic anomaly in the lower troposphere over the SC–East China Sea region, and the SC-pattern rainfall anomalies are caused by the anticyclonic anomaly over the northern SCS and the Philippine Sea. The physical processes responsible for the formation of the two cyclonic and anticyclonic anomalies in the lower troposphere are discussed in the following subsections 5.2 and 5.3, respectively.

5.2. *Extratropical impact on the SS pattern*

The lower-tropospheric cyclonic anomaly over the SC–East China Sea region, in the positive phase of the SS pattern, is connected with an extratropical wave train originating from the mid–high latitudes of the North Atlantic in the upper troposphere (Fig. 10a). To reveal the characteristics of the associated Rossby wave propagation, the zonal and meridional components of a wave-activity flux for stationary Rossby waves ($\boldsymbol{W}$) are employed, following Takaya and Nakamura (2001), which is defined as

$$\boldsymbol{W} = \frac{1}{2|\overline{\boldsymbol{V}}|}\begin{pmatrix} \overline{u}(\psi_x'^2 - \psi'\psi'_{xx}) + \overline{v}(\psi'_x\psi'_y - \psi'\psi'_{xy}) \\ \overline{u}(\psi'_x\psi'_y - \psi'\psi'_{xy}) + \overline{v}(\psi_y'^2 - \psi'\psi'_{yy}) \end{pmatrix},$$

where $|\boldsymbol{V}|$ is the magnitude of the horizontal vector wind (u, v) and ψ is the stream function. Variables with an overbar represent their climatological summer mean averaged during

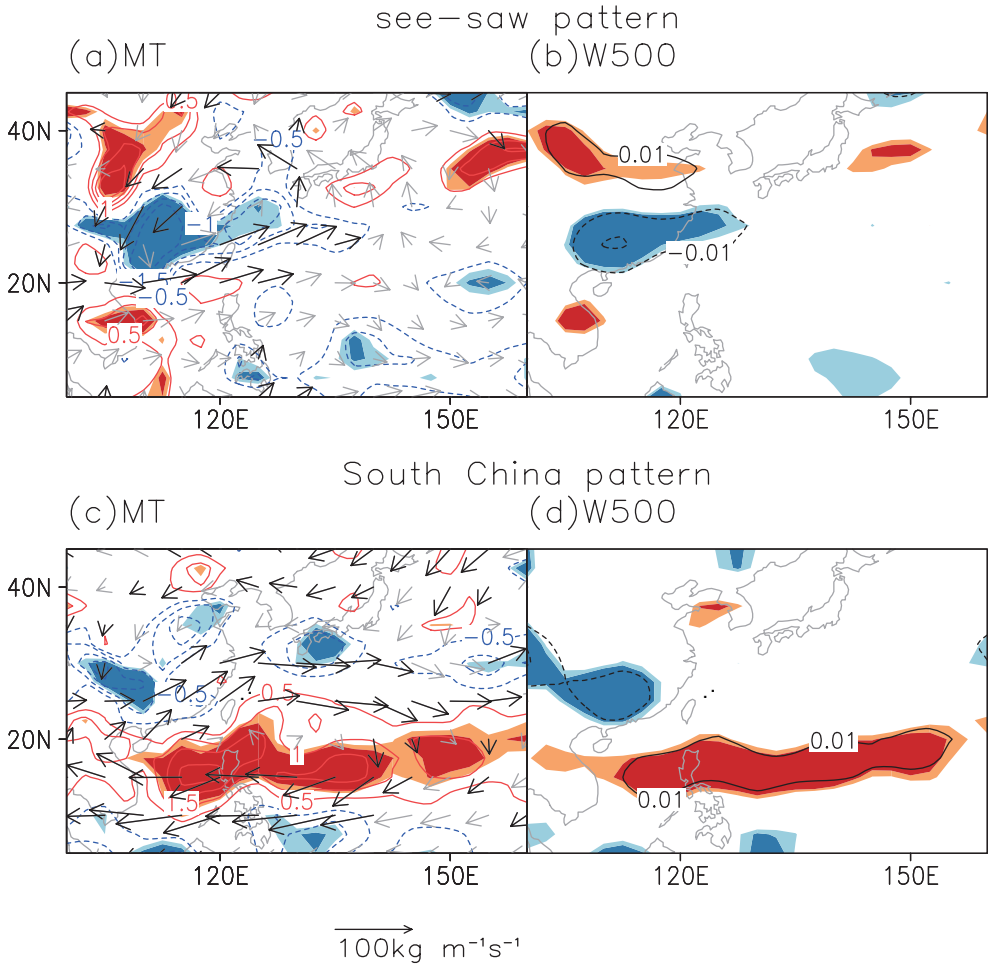

Fig. 9. As in Figs. 6c and f but for the composite results of interannual anomalies of column (a, c) moisture transport (vectors), which is vertically integrated from 300 hPa to the surface, and its divergence (contours) and (b, d) vertical pressure velocity at 500 hPa. Statistically significant moisture transport anomalies at the 95% confidence level are plotted with bold vectors in (a, c), and the units are given at the bottom of (c). Dark and light shading indicates statistically significant anomalies at the 95% and 90% confidence levels, respectively. The contour interval is 0.5 mm d^{-1} in (a, c) and 0.01 Pa s^{-1} in (b, d).

1951–2011, and variables with subscript and prime notations signify their partial derivatives and anomalies associated with the SS pattern.

The wave-activity flux at 200 hPa, related to the wave train, originates in the mid–high latitudes of the North Atlantic, extends eastward into northern Europe, and then diverts over central Asia at approximately 60°E southeastward into the Asian westerly jet (Fig. 10b). Subsequently, it continues to propagate eastward into East Asia along the Asian westerly jet, causing a negative geopotential height at 200 hPa over East Asia. A similar spatial distribution of geopotential height at 850 hPa (H850) is also revealed (Fig. 10c), suggesting a barotropic nature of the extratropical wave train. The cyclonic anomaly over the SC–East China Sea region in the lower troposphere is formed as the barotropic response to the negative upper-tropospheric geopotential height over East Asia.

The external forcing related to the SS pattern is also examined. The composite sea surface temperature (SST) anomalies show no significant signal in the tropical oceans and the North Atlantic in the concurrent summer (figure not shown).

5.3. *Effect of the WNP heating on the SC pattern*

The anticyclonic anomaly, responsible for enhanced rainfall over SC in the SC pattern, is associated with a rainfall decrease over the northern SCS and the Philippine Sea, based on the composite GPCP precipitation difference of the three cases in the positive phase, and three cases in the negative phase of the SC pattern since 1979 (Table 2). The decrease in rainfall over the SCS and the Philippine Sea is also supported by the composite results using the NCEP–NCAR reanalysis precipitable water data during 1951–2011 (Fig. 11b). The rainfall reduction–related descent (Fig. 11c) causes an anticyclonic anomaly over the northern SCS and the Philippine Sea, through divergence near the surface with friction. Mean-

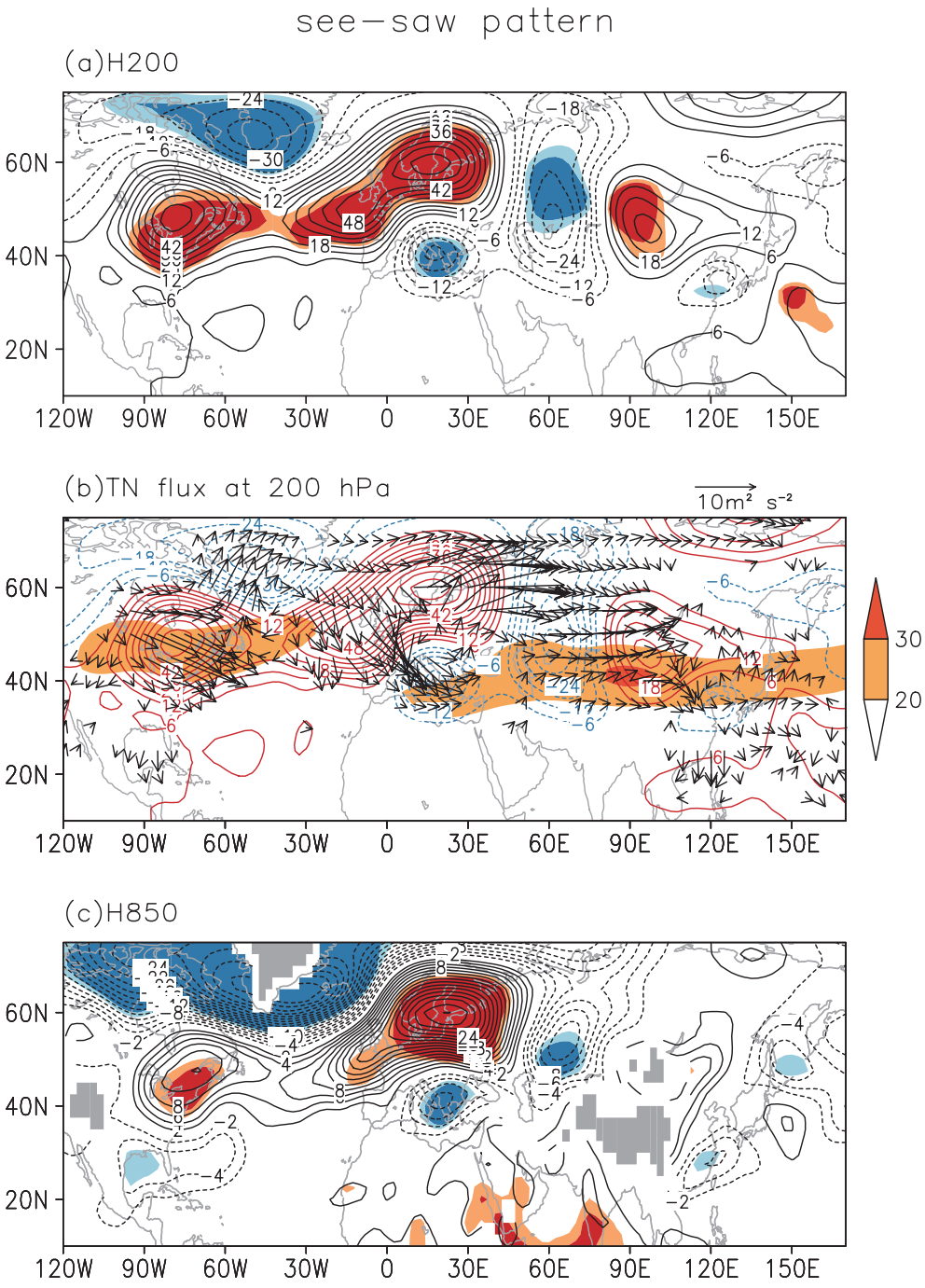

Fig. 10. As in Fig. 6c but for the composite results of (a) interannual anomalies of geopotential height and (b) associated Takaya and Nakamura flux (vectors) at 200 hPa, and (c) geopotential height at 850 hPa. Dark and light shading indicates statistically significant anomalies at the 95% and 90% confidence levels in (a, c). Shading in (b) depicts the location of the climatological westerly jet at 200 hPa. The contour interval is 6 gpm in (a, b) and 2 gpm in (c). The effect of the topography is masked by grey shading in (c).

while, the reduced rainfall–related WNP heating sink may excite a Rossby wave response in the west (Gill, 1980), further enhancing the anticyclonic anomaly (Lu, 2001; Lu and Lin, 2009).

The SST related to the SC pattern warms in the Bay of Bengal, the SCS, and the Philippine Sea (Fig. 11d). The reduced rainfall over the warm SST anomalies suggests that the SST anomalies are a response against the anticyclonic anomaly related to the SC pattern. The anticyclonic anomaly may increase incoming shortwave radiation into the underlying oceans because of cloud cover reduction related to the suppressed rainfall. It may also suppress the Asian monsoon westerly in the south, reducing surface evaporation such that the SST warms.

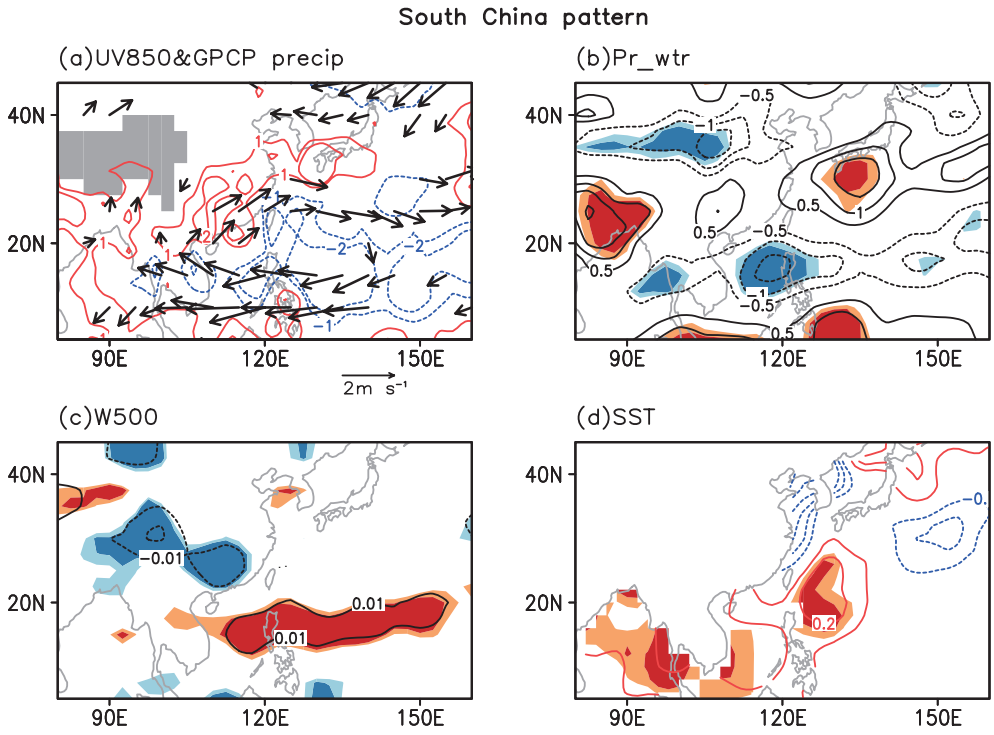

Fig. 11. As in Fig. 6f but for the composite results of interannual summer anomalies of (a) horizontal winds at 850 hPa (vectors) and GPCP precipitation (contours), (b) NCEP–NCAR reanalysis precipitable water for the entire atmosphere, (c) vertical pressure velocity at 500 hPa, and (d) SST. Dark and light shading indicates statistically significant anomalies at the 95% and 90% confidence levels, respectively. The contour interval is 1 mm d^{-1} in (a), 0.5 kg m^{-2} in (b), 0.01 Pa s^{-1} in (c), and 0.1°C in (d). The effect of the topography is masked by grey shading in (a).

It is also noted that the WNP sinking-induced Rossby wave further propagates northeastward (Fig. 11a), resembling the PJ pattern (Nitta, 1987) or the EAP pattern (Huang and Sun, 1992). Some previous studies have revealed that the EOF1 mode is also affected by the EAP pattern triggered by the WNP heating (e.g. Huang et al., 2007). To distinguish their difference, Fig. 12 shows the regions with significant positive H850 anomalies related to the SC pattern and the EOF1 mode, separately. The significant H850 anomalies related to the SC pattern cover the SCS and Philippine Sea, while the anomalies related to the EOF1 mode expand northward, further covering the SC region. The different H850 responses to the WNP heating are possibly due to the change in the basic state, since monsoon rainfall peaks in June over SC and in June–July over the Yangtze River valley. This requires further investigation in future work. The northward expansion of the H850 anomalies causes the northward shift of the associated southwesterly anomaly and moisture transport in the west from SC to the Yangtze River valley. Consequently, rainfall increases in SC associated with the SC pattern, and in the Yangtze River valley associated with the EOF1 mode.

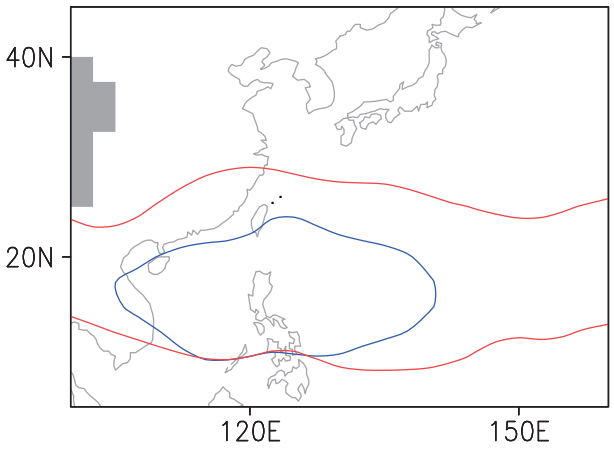

Fig. 12. The regions with statistically significant geopotential height at 850 hPa at the 95% confidence level related to the EOF1 mode (surrounded by the red contour) and the SC pattern (blue contour). The effect of the topography is masked by grey shading.

6. Conclusion and discussion

In this study, the authors reveal the EOF2 mode of interannual summer rainfall anomalies depicts a meridional shift of the YRRB. Moreover, the meridional shift of the YRRB is mostly due to two different types of rainfall anomaly patterns: one that reflects an SS pattern of rainfall anomalies between the YH and SC, and the other with the main rainfall anomalies concentrated in SC. The first pattern is referred to as the SS pattern and the latter is called the SC pattern. There are 13

SS-pattern years and 16 SC-pattern years, which account for three quarters of the total 39 strong EOF2-mode years during 1951–2011. Corresponding to a southward shift of the YRRB, rainfall increases in SC and decreases in the YH in the SS pattern, and it increases in SC only in the SC pattern.

The SS and SC patterns are related to different circulation anomalies. The SS pattern is associated with a lower-tropospheric cyclonic anomaly over SC and the East China Sea, with the northerly anomaly blowing from the YH to SC, weakening the climatological monsoon southwesterly. The weakened monsoon suppresses northward moisture transport and subsequent rainfall in the north, i.e., over the YH, and enhances rainfall in the south over SC. The SC pattern is, however, mainly related to an anticyclonic anomaly over the northern SCS and the Philippine Sea, suggesting a westward extension of the WNPSH. The enhanced southwesterly in the west transports more moisture to SC and favors rainfall.

Moreover, two different mechanisms responsible for the formation of the cyclonic anomaly related to the SS pattern and the anticyclonic anomaly related to the SC patterns are proposed. The SS pattern results from an extratropical wave train originated from the mid–high latitudes of the North Atlantic. The wave train extends eastward into northern Europe, diverts over central Asia, at approximately 60°E, southeastward into the Asian westerly jet, and then propagates eastward to finally reach East Asia and cause a near-barotropic cyclonic anomaly over SC and the East China Sea. For the SC pattern, the anticyclonic anomaly over the northern SCS and the Philippine Sea is related to the suppressed rainfall in the WNP.

The present study carefully examines the EOF2 mode of interannual summer rainfall in East China and reveals two different rainfall patterns in the EOF2 mode, with nearly equivalent numbers of cases (13 SS-pattern cases and 16 SC-pattern cases). The SS pattern reflects a dipole-like pattern with opposite rainfall variation in the YH and SC, and the SC pattern represents a monopole-like pattern with rainfall anomalies concentrated in SC. The existence of the monopole-like SC pattern associated with the EOF2 mode may challenge the traditional view of the "dipole" mode of summer rainfall in East China (Zhu and Chen, 1992; Shen and Lau, 1995; You et al., 2003; Zhou and Yu, 2005; Chen et al., 2006). Instead, in this study, we propose that the EOF2 mode may better depict the latitudinal variation of the summer-mean YRRB.

We identify two main rainfall patterns associated with the EOF2 mode: the SS and SC patterns. It is interesting to note that there is no YH pattern, in which rainfall anomalies are concentrated in the YH only. In the 39 strong EOF2-mode years, there are only five years with strong rainfall anomalies in the YH and normal rainfall in SC (Table 2), far fewer than the 13 SS-pattern years and 16 SC-pattern years. The absence of the YH pattern is likely due to the much smaller interannual variance of summer rainfall in the YH than SC explained by the EOF2 mode (Fig. 2).

The structure of the composite rainfall anomalies in the positive (Fig. 6d) and negative (Fig. 6e) phases of the SC pattern slightly deviate from their composite difference in Fig. 6f, though they are basically opposite. The deficient rainfall in SC in the negative phase deviates southeastward and the sufficient rainfall in the positive phase deviates northwestward. The nonlinearity indicated by the different deviation from the range is probably due to the different zonal extension of the WNPSH (Fig. 8f). Under the control of the westward-extended WNPSH, anomalous moisture transport by the southwesterly anomaly in the west shifts northwestward in the positive phase (figure not shown), while that transported by the northeasterly anomaly shifts southeastward under the eastward-retreated WNPSH in the negative phase (figure not shown). Accordingly, the rainfall anomalies move northwestward in the positive phase and southeastward in the negative phase.

Han and Zhang (2009) investigated anomalies related to the EOF2 mode of summer rainfall in East China. They proposed that the mode, with increasing rainfall to the south of the Yangtze River over SC and decreasing rainfall to the north over the YH, is induced by a southwestward extension of the WNPSH. In this study, we show that the westward extension of the WNPSH only contributes to the increased rainfall in SC. The opposite change in summer rainfall between the YH and SC (the SS pattern), with above-normal rainfall in SC and below-normal rainfall in the YH, is related to a cyclonic anomaly over SC and the adjacent East China Sea, which is probably affected by the extratropical wave train originated from the mid–high latitudes of the North Atlantic.

Acknowledgements. The authors appreciate the editor's and the two reviewers' comments and suggestions, which led to an improved manuscript. This research was supported by the National Natural Science Foundation of China (Grant Nos. 41375086 and 41320104007).

REFERENCES

Adler, R. F., and Coauthors, 2003: The version-2 global precipitation climatology project (GPCP) monthly precipitation analysis (1979–present). *J. Hydrometeor.*, **4**, 1147–1167.

Chen, J. L., and R. H. Huang, 2007: The comparison of climatological characteristics among Asian and Australian monsoon subsystems. Part II: Water vapor transport by summer monsoon. *Chinese J. Atmos. Sci.*, **31**, 766–778. (in Chinese)

Chen, W., L. H. Kang, and D. Wang, 2006: The coupling relationship between summer rainfall in China and global sea surface temperature. *Climatic and Environmental Research*, **11**, 259–269. (in Chinese)

Ding, Y. H., and J. C. L. Chan, 2005: The East Asian summer monsoon: An overview. *Meteor. Atmos. Phys.*, **89**, 117–142.

Gill, A. E., 1980: Some simple solutions for heat-induced tropical circulation. *Quart. J. Roy. Meteor. Soc.*, **106**, 447–462.

Han, J. P., and R. H. Zhang, 2009: The dipole mode of the summer rainfall over East China during 1958–2001. *Adv. Atmos. Sci.*, **26**, 727–735, doi: 10.1007/s00376-009-9014-6.

He, M., and X. Li, 1992: The relationship between summer rainfall in China and tropical circulation anomaly. *Quarterly Journal of Applied Meteorology*, **3**, 181–189. (in Chinese)

Huang, R. H., and F. Y. Sun, 1992: Impacts of the tropical western Pacific on the East Asian summer monsoon. *J. Meteor. Soc. Japan*, **70**, 243–256.

Huang, R. H., Y. H. Xu, and L. T. Zhou, 1999: The inter-decadal variation of summer precipitations in China and the drought trend in North China. *Plateau Meteorology*, **18**, 465–476. (in Chinese)

Huang, R. H., L. T. Zhou, and W. Chen, 2003: The progresses of recent studies on the variabilities of the East Asian monsoon and their causes. *Adv. Atmos. Sci.*, **20**, 55——69, doi: 10.1007/BF03342050.

Huang, R. H., J. L. Chen, G. Huang, and Q. L. Zhang, 2006: The quasi-biennial oscillation of summer monsoon rainfall in China and its cause. *Chinese J. Atmos. Sci.*, **30**, 545–560. (in Chinese)

Huang, R. H., J. L. Chen, and G. Huang, 2007: Characteristics and variations of the East Asian monsoon system and its impacts on climate disasters in China. *Adv. Atmos. Sci.*, **24**, 993–1023, doi: 10.1007/s00376-007-0993-x.

Huang, R. H., J. L. Chen, L. Wang, and Z. D. Lin, 2012: Characteristics, processes, and causes of the spatio-temporal variabilities of the East Asian monsoon system. *Adv. Atmos. Sci.*, **29**, 910–942, doi: 10.1007/s00376-012-2015-x.

Huffman, G. J., and Coauthors, 1997: The global precipitation climatology project (GPCP) combined precipitation dataset. *Bull. Amer. Meteor. Soc.*, **78**, 5–20.

Kalnay, E., and Coauthors, 1996: The NCEP/NCAR 40-year reanalysis project. *Bull. Amer. Meteor. Soc.*, **77**, 437–471.

Lau, K.-M., K.-M. Kim, and S. Yang, 2000: Dynamical and boundary forcing characteristics of regional components of the Asian summer monsoon. *J. Climate*, **13**, 2461–2482.

Lu, R.Y., 2001: Interannual variability of the summertime North Pacific subtropical high and its relation to atmospheric convection over the warm pool. *J. Meteor. Soc. Japan*, **79**, 771–783.

Lu, R. Y., 2004: Associations among the components of the East Asian summer monsoon system in the meridional direction. *J. Meteor. Soc. Japan*, **82**, 155–165.

Lu, R. Y., and Z. D., Lin, 2009: Role of subtropical precipitation anomalies in maintaining the summertime meridional teleconnection over the western North Pacific and East Asia. *J. Climate*, **22**, 2058–2072.

Nitta, T., 1987: Convective activities in the tropical western Pacific and their impact on the Northern Hemi sphere summer circulation. *J. Meteor. Soc. Japan*, **64**, 373–390.

North, G. R., T. Bell, R. F. Cahalan, and F. J. Moeng, 1982: Sampling errors in the estimation of empirical orthogonal functions. *Mon. Wea. Rev.*, **110**, 699–706.

Shen, B. Z., Z. D. Lin, R. Y. Lu, and Y. Lian, 2011: Circulation anomalies associated with interannual variation of early-and late-summer precipitation in Northeast China. *Science China Earth Sciences*, **54**, 1095–1104.

Shen, S., and K. M. Lau, 1995: Biennial oscillation associated with the East Asian summer monsoon and tropical sea surface temperatures. *J. Meteor. Soc. Japan*, **73**, 105–124.

Smith, T. M., R. W. Reynolds, T. C. Peterson, and J. Lawrimore, 2008: Improvements to NOAA's historical merged land–ocean surface temperature analysis (1880–2006). *J. Climate*, **21**, 2283–2296.

Su, Q., R. Y. Lu, and C. F. Li, 2014: Large-scale circulation anomalies associated with interannual variation in monthly rainfall over South China from May to August. *Adv. Atmos. Sci.*, **31**, 273–282, doi: 10.1007/s00376-013-3051-x.

Takaya, K., and H. Nakamura, 2001: A formulation of a phase-independent wave-activity flux for stationary and migratory quasigeostrophic eddies on a zonally varying basic flow. *J. Atmos. Sci.*, **58**, 608–627.

Wang, B., R. G. Wu, and K. M. Lau, 2001: Interannual variability of the Asian summer monsoon: Contrasts between the Indian and the western North Pacific-East Asian monsoons. *J. Climate*, **14**, 4073–4090.

Weng, H. Y., K. M. Lau, and Y. K. Xue, 1999: Multi-scale summer rainfall variability over China and its long-term link to global sea surface temperature variability. *J. Meteor. Soc. Japan*, **77**, 845–857.

Wu, R. G., Z. P. Wen, S. Yang, and Y. Q. Li, 2010: An interdecadal change in southern China summer rainfall around 1992/93. *J. Climate*, **23**, 2389–2403.

Ye, H., and R. Y. Lu, 2012: Dominant patterns of summer rainfall anomalies in East China during 1951–2006. *Adv. Atmos. Sci.*, **29**, 695–704, doi: 10.1007/s00376-012-1153-5.

You, Y., Y. Zhou, X. Yang, and L. Fang, 2003: Using EOF method to analysis the spatial distribution and temporal variation of summer rainfall in China. *Journal of Sichuan Meteorology*, **23**, 22–23. (in Chinese)

Zhou, T.-J., and R.-C. Yu, 2005: Atmospheric water vapor transport associated with typical anomalous summer rainfall patterns in China. *J. Geophys. Res.*, **110**, D08104, doi: 10.1029/2004JD005413.

Zhu, Q. G., and X. G. Chen, 1992: Objective division of natural rainfall regions in China. *Journal of Nanjing Institute of Meteorology*, **15**, 467–475. (in Chinese)

Zou, L., and Y. Q. Ni, 1998: Impact of ENSO on the variability of the summer monsoon over Asia and the summer rainfall in China. *Journal of Tropical Meteorology*, **13**, 306–314. (in Chinese)